Supporting Information

A QM/MM Study of the Bergman Reaction of Dynemicin A in the Minor Groove of DNA

Tell Tuttle[†], Elfi Kraka,[‡] Walter Thiel[†] and Dieter Cremer[*‡]*

Max-Planck-Institut für Kohlenforschung, D-45470 Mülheim an der Ruhr, Germany; Department of Chemistry and Department of Physics, University of the Pacific, 3601 Pacific Avenue, Stockton, California 95211-0110

Email: thiel@mpi-muelheim.mpg.de (W.T.), dcremer@pacific.edu (D.C.)

[†] Max-Planck-Institut für Kohlenforschung

[‡] University of the Pacific

List of Contents

1. Computational details

Gas phase calculations. The Bergman cyclization in both model and naturally occurring compounds is well described by density functional theory (DFT). DFT accounts for long-range correlation effects through the local exchange potential and, in an unspecified way, through the inherent self-interaction error.[1-4] The use of broken-symmetry unrestricted DFT (BS-UDFT) specifically incorporates long-range correlation into the calculation and thus the choice of the functional is dictated by the need to avoid double counting of the correlation effects.[5,6] The B3LYP functional[7-11] in connection with either the 3-21G[12] or 6-31G(d,p)[13] basis set satisfies this requirement and therefore these combinations were used for the optimization of all structures in the gas phase. The calculations in the gas phase were performed in Gaussian03.[14]

System preparation, classical simulations. There is no experimentally determined structure for dynemicin A complexed with DNA. Therefore, we constructed a duplex 10-mer B-DNA sequence with the same primary sequence – d(CTACTACTGG) – that has previously been used.[15] All fully classical calculations (including: hydration of the system, molecular mechanics (MM) minimizations and MD simulations) were carried out with the CHARMM program.[16-18] The DNA segment was minimized and the gas-phase optimized anionic dynemicin ligand (**2**) was docked into the minor groove of the segment using AutoDock[19,20] in the same manner as previously described for the neutral ligand.[15]

The system was neutralized by the addition of counterions (Mg^{2+}/Na^{+}) around the **2**-DNA complex. One Mg^{2+} ion was placed at each end of the duplex, to satisfy the -2 charge of the two terminal residues. Na^{+} ions were then positioned opposite to each of the PO_4^{-} groups along the backbone (18 in total). Finally, the Na^{+} ion closest to the COO^{-}

group of the ligand was converted into a Mg^{2+} ion, yielding a total system charge of 0. The neutral system thus obtained was solvated by a sphere of TIP3P waters[21] of radius 30 Å, centered about the geometric center of the bound ligand. All waters that overlapped[22] with the complex were deleted.

The system was minimized for 500 Steepest Descent steps, followed by 10,000 ABNR (Adopted Basis Newton Raphson) steps,[17] and subsequently equilibrated for 1ns at 310K using Langevin Dynamics with a 1 fs time-step. The SHAKE algorithm[23] was employed for all bonds involving hydrogen. A stochastic boundary potential[24] was used to maintain the structure of the water sphere during the MD simulation. In both the CHARMM minimization and subsequent equilibration the structure of **2** was kept fixed. The standard CHARMM force field[25-28] does not contain parameter or topology data for the dynemicin A ligand; therefore, the MM parameters and topology of dynemicin A were automatically generated with QUANTA98 using the CHARMm forcefield.[29] While these parameters are not strictly compatible with the academic version of CHARMM, the restraining of the ligand geometry ensures that only the van der Waals parameters and partial charges are important during the MM minimization and equilibration. To this end, the parameterization of the ligand was considered sufficient.

The RMSD for the DNA atoms of the final structure relative to the minimized DNA is 1.3 Å. In addition we observed that the H-bond network between the DNA bases was conserved, with only minor deviations for the terminal base pairs. The counterions remained associated to the charge groups to which they were assigned and the development of solvent shells around the charged species was evident. The reproduction of these qualitative features as well as the acceptable RMSD for the DNA structure

indicate that the final system is well equilibrated and therefore provides a reasonable starting point for the QM/MM optimization.

QM/MM setup. The QM region is electronically coupled to the MM region by including the point charges from the environment into the one electron QM Hamiltonian (see the main text for the definition of QM and MM regions). In an attempt to increase the efficiency of the calculations, a cutoff of 15 Å was initially applied for the inclusion of point charges. However, this approach led to a fluctuating number of point charges entering the Hamiltonian, which resulted in inconsistent absolute energies between the stationary points. Thus, for all results reported no QM/MM cutoff was applied.

The QM/MM geometry optimizations were performed with HDLC_OPT – a linear scaling, microiterative algorithm that employs a set of hybrid delocalized coordinates – as implemented in CHEMSHELL.[30-32] The residues defined for this optimization procedure were taken as the standard residues defined for CHARMM (e.g. nucleic acids, waters, dynemicin).

In QM/MM optimizations of complex large systems, it is important to ensure the connectivity between the reactants, products, and the associated transition states (TS). To achieve this goal, we first located **TS(2-3)** and performed a frequency calculation on the QM region of the optimized structure, at the QM/MM level. The presence of a single imaginary frequency corresponding to the reaction coordinate confirmed that the correct TS had been found. The ligand was then shifted slightly towards the reactant (product) side, and the structure was then optimized to attain **2** (**3**). Starting from the optimized structure of **3-T,** the geometry was altered towards that of **TS(3-4)** and optimized to locate **TS(3-4)** whose correct nature was again verified by a frequency calculation.

Finally, the geometry was modified slightly towards **4** and then fully optimized to obtain the structure of the product. Using this procedure, we have established that a contiguous path connects the minima and transition states during the reactions studied.

Approximating the singlet biradical. The optimization of the singlet biradical was extremely time-consuming, due primarily to the necessity of using a quadratically convergent SCF routine. Therefore, we tested the validity of using the optimized structure of the triplet (**3-T**) to calculate the energy of the singlet (**3-S**).

Table S1. Comparison of geometries and relative energies for **3-S** and **3-T**.[a]

	ΔE	C23-C24	C24-C25	C25-C26	C26-C27	C27-C28	C28-C23
3-S	0.0 (3.3)	1.377	1.373	1.429	1.373	1.376	1.430
3-T	2.8 (0.4)	1.383	1.381	1.414	1.381	1.385	1.414

[a]Energies in kcal/mol relative to the energy of the optimized singlet biradical; bond lengths in Å (see Scheme 1 of the paper for atom numbering). Structures optimized at the B3LYP/3-21G level. Values in parentheses correspond to a single point calculation of the structure using the alternative electronic state.

In Table S1, we compare the bond lengths of the optimized triplet and singlet biradical warheads, along with the relative energies of the structures. In addition, the destabilization resulting from using the geometry of one optimized electronic structure to calculate the other electronic state is also given. The most accurate singlet-triplet (S-T) splitting results from the energy difference of the structures (ΔE(S-T) = 2.8 kcal/mol) when optimized in the correct electronic states (i.e. **3-S** and **3-T**). However, the bond distances within the *p*-benzyne warhead are similar in the singlet and triplet optimized structures as has been discussed in the literature. There is a slight elongation (< 0.01 Å) of

the bonds involving the radical carbon atoms (C24 and C27) for the **3-T** structure. Conversely, the remote C-C bonds are slightly shorter (≈ 0.015 Å). These geometric changes are small, as reflected in the energy difference between the optimized singlet and the singlet at the optimized triplet geometry (ΔE = 0.4 kcal/mol). The alternative case of using the triplet at the optimized singlet geometry causes an increase in the S-T splitting by a similar amount (ΔΔE = 0.5 kcal/mol) due to the further destabilization of the triplet through using a non-optimized geometry. These minor energy changes indicate that the use of the optimized triplet geometry in determining the S-T splitting is a justified approximation. As such, during the QM/MM optimization of the Bergman cyclization reaction the singlet biradical system was calculated at the optimized triplet geometry.

References

(1) Polo, V.; Gräfenstein, J.; Kraka, E.; Cremer, D. *Theor. Chem. Acc.* **2003**, *109*, 22.
(2) Polo, V.; Gräfenstein, J.; Kraka, E.; Cremer, D. *Chem. Phys. Lett.* **2002**, *352*, 469.
(3) Polo, V.; Kraka, E.; Cremer, D. *Mol. Phys.* **2002**, *100*, 1771.
(4) Polo, V.; Kraka, E.; Cremer, D. *Theor. Chem. Acc.* **2002**, *107*, 291.
(5) Gräfenstein, J.; Kraka, E.; Cremer, D. *Phys. Chem. Chem. Phys.* **2004**, *6*, 1096.
(6) Gräfenstein, J.; Kraka, E.; Cremer, D. *J. Chem. Phys.* **2004**, *120*, 524.
(7) Becke, A. D. *J. Chem. Phys.* **1993**, *98*, 5648.
(8) Becke, A. D. *Phys. Rev. A* **1988**, *38*, 3098.
(9) Hertwig, R. H.; Koch, W. *Chem. Phys. Lett.* **1997**, *268*, 345.
(10) Lee, C. T.; Yang, W. T.; Parr, R. G. *Phys. Rev. B* **1988**, *37*, 785.
(11) Stephens, P. J.; Devlin, F. J.; Chabalowski, C. F.; Frisch, M. J. *J. Phys. Chem.* **1994**, *98*, 11623.
(12) Binkley, J. S.; Pople, J. A.; Hehre, W. J. *J. Am. Chem. Soc.* **1980**, *102*, 939.
(13) Hariharan, P. C.; Pople, J. A. *Theor. Chim. Acta* **1973**, *28*, 213.
(14) Frisch, M. J.; Trucks, G. W.; Schlegel, H. B.; Scuseria, G. E.; Robb, M. A.; Cheeseman, J. R.; Montgomery, J., J. A.; Vreven, T.; Kudin, K. N.; Burant, J. C.; Millam, J. M.; Iyengar, S. S.; Tomasi, J.; Barone, V.; Mennucci, B.; Cossi, M.; Scalmani, G.; Rega, N.; Petersson, G. A.; Nakatsuji, H.; Hada, M.; Ehara, M.; Toyota, K.; Fukuda, R.; Hasegawa, J.; Ishida, M.; Nakajima, T.; Honda, Y.; Kitao, O.; Nakai, H.; Klene, M.; Li, X.; Knox, J. E.; Hratchian, H. P.; Cross, J. B.; Bakken, V.; Adamo, C.; Jaramillo, J.;

Gomperts, R.; Stratmann, R. E.; Yazyev, O.; Austin, A. J.; Cammi, R.; Pomelli, C.; Ochterski, J. W.; Ayala, P. Y.; Morokuma, K.; Voth, G. A.; Salvador, P.; Dannenberg, J. J.; Zakrzewski, V. G.; Dapprich, S.; Daniels, A. D.; Strain, M. C.; Farkas, O.; Malick, D. K.; Rabuck, A. D.; Raghavachari, K.; Foresman, J. B.; Ortiz, J. V.; Cui, Q.; Baboul, A. G.; Clifford, S.; Cioslowski, J.; Stefanov, B. B.; Liu, G.; Liashenko, A.; Piskorz, P.; Komaromi, I.; Martin, R. L.; Fox, D. J.; Keith, T.; Al-Laham, M. A.; Peng, C. Y.; Nanayakkara, A.; Challacombe, M.; Gill, P. M. W.; Johnson, B.; Chen, W.; Wong, M. W.; Gonzalez, C.; Pople, J. A. *Gaussian 03 Revision C.01*, Gaussian, Inc.; Wallingford, CT, 2004

(15) Tuttle, T.; Kraka, E.; Cremer, D. *J. Am. Chem. Soc.* **2005**, *127*, 9469.

(16) *CHARMM*, V. c31b1, 2004

(17) Brooks, B. R.; Bruccoleri, R. E.; Olafson, B. D.; States, D. J.; Swaminathan, S.; Karplus, M. *J. Comput. Chem.* **1983**, *4*, 187.

(18) MacKerell, A. D.; Brooks, B. R.; Brooks, C. L., III; Nilsson, L.; Roux, B.; Won, Y.; Karplus, M. In *Encyclopedia of Computational Chemistry*; Schleyer, P. v. R., Ed.; Wiley: Chichester, 1998; Vol. 1, p 271.

(19) Morris, G. M.; Goodsell, D. S.; Halliday, R. S.; Huey, R.; Hart, W. E.; Belew, R. K.; Olson, A. J. *J. Comput. Chem.* **1998**, *19*, 1639.

(20) Morris, G. M.; Goodsell, D. S.; Huey, R.; Olson, A. J. *J. Comput.-Aided Mol. Des.* **1996**, *10*, 293.

(21) Jorgensen, W. L.; Chandrasekhar, J.; Madura, J. D.; Impey, R. W.; Klein, M. L. *J. Chem. Phys.* **1983**, *79*, 926.

(22) Overlapping is defined by the distance between the TIP3P oxygen atom and any non-TIP3P heavy atom: R(O-X). If R(O-X) < 2.8 Å the TIP3P water is deleted.

(23) Ryckaert, J. P.; Ciccotti, G.; Berendsen, H. J. C. *J. Comput. Phys.* **1977**, *23*, 327.

(24) Brooks, C. L.; Karplus, M. *J. Chem. Phys.* **1983**, *79*, 6312.

(25) Foloppe, N.; MacKerell, A. D. *J. Comput. Chem.* **2000**, *21*, 86.

(26) MacKerell, A. D.; Banavali, N.; Foloppe, N. *Biopolymers* **2000**, *56*, 257.

(27) MacKerell, A. D.; Banavali, N. K. *J. Comput. Chem.* **2000**, *21*, 105.

(28) MacKerell, A. D.; Bashford, D.; Bellott, M.; Dunbrack, R. L.; Evanseck, J. D.; Field, M. J.; Fischer, S.; Gao, J.; Guo, H.; Ha, S.; Joseph-McCarthy, D.; Kuchnir, L.; Kuczera, K.; Lau, F. T. K.; Mattos, C.; Michnick, S.; Ngo, T.; Nguyen, D. T.; Prodhom, B.; Reiher, W. E.; Roux, B.; Schlenkrich, M.; Smith, J. C.; Stote, R.; Straub, J.; Watanabe, M.; Wiorkiewicz-Kuczera, J.; Yin, D.; Karplus, M. *J. Phys. Chem. B* **1998**, *102*, 3586.

(29) Momany, F. A.; Rone, R. *J. Comput. Chem.* **1992**, *13*, 888.

(30) *ChemShell*, V. 3.0a3, 2004

(31) Billeter, S. R.; Turner, A. J.; Thiel, W. *Phys. Chem. Chem. Phys.* **2000**, *2*, 2177.

(32) Sherwood, P.; de Vries, A. H.; Guest, M. F.; Schreckenbach, G.; Catlow, C. R. A.; French, S. A.; Sokol, A. A.; Bromley, S. T.; Thiel, W.; Turner, A. J.; Billeter, S.; Terstegen, F.; Thiel, S.; Kendrick, J.; Rogers, S. C.; Casci, J.; Watson, M.; King, F.; Karlsen, E.; Sjovoll, M.; Fahmi, A.; Schafer, A.; Lennartz, C. *J. Mol. Struct. (THEOCHEM)* **2003**, *632*, 1.

2. Gas phase calculations with larger basis sets

For the purpose of checking whether a larger basis set or the inclusion of diffuse functions would significantly affect the results of the anionic species we carried out B3LYP calculations with the 6-31G(d,p) and 6-31+G(d,p) basis sets. Results are summarized and compared with B3LYP/3-21G energies in Table S2.

Table S2. Effect of basis set size on the energy profile for anionic dynemicin A.[a]

	ΔE			μ[b]		
	3-21G	**6-31G(d,p)**	**6-31+G(d,p)**	**3-21G**	**6-31G(d,p)**	**6-31+G(d,p)**
2	0.0	0.0	0.0	15.0	16.6	17.1
TS(2-3)	20.4	20.4	20.5	14.7	16.6	17.1
3-S	-0.8	-3.2	-1.9	15.0	16.6	17.2
3-T	2.0	-1.1	0.3	15.0	16.6	17.2
TS(3-4)	22.1	24.5	24.3	14.8	16.4	17.0
4	-9.1	-6.7	-7.0	14.9	16.5	17.1

[a]Energies in kcal/mol, dipole moments in Debye. The 6-31+G(d,p) calculations were performed as single point calculations on the 6-31G(d,p) optimized structures.

[b]The origin for the dipole moments is taken as the center of nuclear charge.

The calculated activation barriers are largely unchanged when using the larger basis sets. However, the exothermicity of the singlet formation is predicted to be slightly larger with the 6-31G(d,p) basis set (ΔΔE = -2.3 kcal/mol). The second TS, leading to the acyclic enediyne isomer **4** is calculated to be higher by a corresponding amount and the formation of the product is less exothermic. The addition of diffuse functions to the larger basis set has only a minor effect on the relative energies and generally tends to bring the

results into closer agreement with the 3-21G results. As all of the differences in the relative energies are in the order of 2-3 kcal/mol, we consider this as a validation of the usefulness of the 3-21G basis set, in conjunction with the B3LYP functional for studying the Bergman cyclization of the anionic form of dynemicin A.

3. Analysis of interaction energies

In this section the influence of the environment on the reaction sequence **2** → **4** is discussed by a decomposition of calculated interaction energies into individual components.

3.1 Bulk environment interactions. In Table S3 the contributions to the relative MM energy differences, between the optimized stationary points, is given with respect to the three segments – water, DNA and counterions – which comprise the environment. In addition, the MM component of the interaction energy between the ligand (QM) and each of these segments is listed. This MM component represents only the van der Waals interactions between dynemicin A and the environment, as the electrostatic interaction energy is contained within the QM energy term and will be considered subsequently.

Table S3. Variations in the MM interaction energies. [a]

	ΔE				ΔE			
	Ligand	**Water**	**DNA**	**Ions**	**Ligand**	**Water**	**DNA**	**Ions**
	2 → TS(2-3)				**TS(2-3) → 3**			
Water	-0.2	2.3			-0.7	-2.7		
DNA	-0.1	-2.7	0.4		-0.3	1.3	0.5	
Ions	0.0	0.8	0.5	0.6	0.0	-0.7	-1.5	0.3
	3 → TS(3-4)				**TS(3-4) → 4**			
Water	0.2	-3.2			1.9	1.0		
DNA	-0.2	3.1	0.6		-0.5	-0.1	1.6	
Ions	0.0	-1.1	-0.1	0.3	0.0	0.6	-1.3	-0.1

[a]Energies are reported in kcal/mol. Structures optimized at the B3LYP/3-21G//CHARMM level of theory.

The data presented in Table S3 shows that the interaction of the ligand with the environment is relatively consistent (variations of less than 1 kcal/mol) in all cases, except for **4**. In the reaction step moving from **TS(3-4)** to **4** there is a change in the van der Waals interactions between the ligand and the water, which leads to a 1.9 kcal/mol destabilization. However, this destabilization is partially offset by more favorable interactions between the ligand and the DNA (ΔE = -0.5 kcal/mol).

Differences in the solvent sphere account for the largest variations in the MM energies. However, changes in the solvent sphere are generally compensated such that the system as a whole remains stable. For example, in the formation of **TS(2-3)**, the re-orientation of water molecules leads to less favorable water-water interactions (ΔE = 2.3 kcal/mol), while the water-DNA interaction becomes more stabilizing (ΔE = -2.7 kcal/mol). The acyclic enediyne **4** is an exception since the change in the water configuration results in a net destabilization of the system by 3.4 kcal/mol (relative to **TS(3-4)**).

3.2 Electrostatic interactions between selected residues and the ligand. The electrostatic effect of individual residues on the reaction profiles can be assessed by removing the partial charges assigned to a residue in the MM region and then re-calculating the QM/MM energy. The resulting change in the QM energy is a measure of the electrostatic influence of the particular residue on the QM region. The changes caused by the charge deletion influence only the QM component of the reaction energy (column 5 of Table 2), as the van der Waals interactions, and thus the MM component, are unaffected by this procedure.

Table S4 lists the total electrostatic interaction energies of the ligand with strands 1 and 2 of the DNA and with the counterions, as obtained from the charge deletion analysis, and their variation during the reaction. Detailed individual interaction energies are given in Tables S5 and S6 of this summary. It is obvious from Table S4 that the total electrostatic interaction of the anionic ligand is strongly repulsive with DNA and strongly attractive with the counterions, as expected from the formal charges. Proceeding along the reaction path, these electrostatic interactions become progressively less favorable overall (by 1.0-3.9 kcal/mol), mostly due to the increased repulsive interactions with DNA strand 1, which are only partially compensated by the other interactions. One should emphasize however, that these variations remain minor compared with the total interaction energies.

Table S4. Electrostatic interactions between the proximal non-water residues with **2** (ΔE) and their variation along the reaction path (ΔΔE, relative to **2**).[a]

	ΔE	ΔΔE			
	2	**TS(2-3)**	**3**	**TS(3-4)**	**4**
Strand 1	141.1	3.8	2.3	3.8	3.3
Strand 2	158.2	-1.6	0.6	0.6	-0.6
Counterions	-196.2	-1.2	-1.2	-1.6	1.2
Sum	103.1	1.0	1.7	2.8	3.9

[a]The individual effects from the proximal DNA bases considered were summed into two groups based on the strand. The interactions of the individual counterions considered have been summed together. For a complete list of the individual interactions see section 3.3. Relative energies are reported in kcal/mol.

It should be pointed out that the individual electrostatic interaction energies between the ligand and the environmental residues do not sum up to the differences E(QM) - E(QM(gas)//QM/MM from Table 2 of the main paper, for two reasons: First we considered only a selected set of residues and neglected the more remote ones. Second, the charge deletion analysis assumes that the individual interactions are additive, which does not hold strictly because of cooperative effects. The purpose of the present analysis is not to reproduce E(QM) - E(QM(gas)//QM/MM, but to check for specific environmental effects on the reaction profile. We find as our main result that there are no pronounced qualitative effects of this kind.

3.3 DNA and counterions energy decomposition. The counterions and DNA residues within 10 Å of the geometric center of **TS(2-3)** are listed in Tables S5 and S6, respectively, which also provide their electrostatic interaction energies with the ligand in the reactant and their variation during the reaction. Consistent with the anionic nature of the ligand, each of the counter-cations has a stabilizing interaction, while the anionic DNA residues are all strongly destabilizing (17-43 kcal/mol, see Table S6).

Table S5. Electrostatic interaction energies of the surrounding counterions with **2** (ΔE) and their variation along the reaction path (ΔΔE).[a]

Residue	ΔE / R	ΔΔE / R			
	2	**TS(2-3)**	**3**	**TS(3-4)**	**4**
Na6	-27.7/11.17	-1.0/11.07	0.0/11.08	-0.6/11.05	0.1/11.02
Na7	-24.9/12.23	-1.3/12.19	-0.5/12.16	-0.9/12.17	0.3/13.14
Na8	-26.1/14.44	0.2/14.47	-0.4/14.46	0.1/14.47	0.0/14.58
Na16	-37.5/9.21	0.4/9.28	-0.5/9.25	-0.2/9.25	0.3/9.38
Mg17	-80.0/8.00	0.5/8.01	0.2/8.03	0.0/8.01	0.5/8.04

[a] Energies in kcal/mol. R is the distance between the ion and the C30 atom of the ligand in Å (see Scheme 1 of the paper for atom numbering).

Going from **2** to **TS(2-3**) the electrostatic interactions with the proximal counterions have a mixed effect. Two sodium ions are moderately stabilizing, relative to **2** (ΔΔE(Na6,Na7) = -2.3 kcal/mol); however, the remaining three cations have a combined destabilizing effect of 1.1 kcal/mol. For the intermediate (**3**) the interactions with the counterions are again more favorable relative to **2** (ΔΔE = -1.2 kcal/mol), with only Mg17 being slightly destabilizing. The electrostatic stabilization offered by the counterions is maintained in the formation of **TS(3-4)** (ΔΔE = -1.6 kcal/mol), but is lost in the final product (ΔΔE = 0.6 kcal/mol).

The Mg17 ion clearly has the largest effect on the QM energy; however, the position of this ion is essentially constant and thus the relative energy differences between systems are small. The Na8 counterion is actually the closest in terms of the minimum distance to any ligand atom, although it is further from the C30 atom.

For the direct interaction of the counterion with the negative charge on the carboxylate group of the ligand, one expects a correlation between the changes in the distance

between the two atoms and the changes in the relative energies. This is seen for Mg17, which is closest to C30 atom: as the counterion distance to C30 increases, the relative stabilization caused by the counterion decreases. However, for the sodium counterions that are more remote, there is generally no such clear correlation (except for specific cases, see e.g. Na16, **3** vs. **4,** Table S3). One should keep in mind, of course, that the counterions also polarize the electronic structure of the ligand and that this polarization may vary in a non-linear fashion because it depends both on the distance and the screening between the ligand and the counterion.

In an overall assessment, the contributions of the individual counterions to the changes in the reaction energetics are always quite small, especially when compared with the much larger total interaction energy.

Table S6. Electrostatic interaction energies of the surrounding DNA bases with **2** (ΔE) and their variation along the reaction path (ΔΔE). Energies in kcal/mol.

Residue	ΔE	ΔΔE			
	2	**TS(2-3)**	**3**	**TS(3-4)**	**4**
1:THY5	24.5	0.1	0.0	0.2	0.2
1:ADE6	34.4	0.7	0.1	1.0	0.4
1:CYT7	34.0	2.0	0.8	1.9	1.3
1:THY8	26.3	1.1	1.2	0.7	1.2
1:GUA9	21.9	-0.1	0.2	0.0	0.2
1: Total		3.8	2.2	3.8	3.3
2:GUA4	17.7	-0.1	0.0	0.0	-0.1
2:THY5	26.7	-0.4	0.2	0.0	-0.3
2:ADE6	37.3	-0.6	0.0	-0.1	-0.5
2:GUA7	43.8	-0.4	0.5	0.6	0.2
2:THY8	32.7	-0.1	-0.1	0.1	0.1
2: Total		-1.6	0.6	0.6	-0.6

We now consider DNA-ligand interactions (Table S6). Following the reaction path from **2** to **TS(2-3)** leads to less favorable interactions (ΔΔE = 3.8 kcal/mol) between the ligand and strand 1 of the DNA (Table S4). However, these are partially offset by the more favorable interaction of strand 2 with the ligand (ΔΔE = -1.7 kcal/mol). The comparison of electrostatic interactions in **3** and **2** reveals that the interactions with the first DNA strand are also destabilizing (ΔΔE = 2.2 kcal/mol). Moreover, the stabilization of the radical intermediate state resulting from interactions is not as prevalent as in the

case of **TS(2-3)**, with the second DNA strand also causing an increase in the relative energy by 0.6 kcal/mol.

Summing the individual interactions of the residues listed in Table S5 and Table S6 for the formation of **TS(3-4)** and **4**, relative to **2**, leads to a destabilization of 0.8 and 3.9 kcal/mol, respectively. The larger destabilization of **4** arises predominantly from less favorable interactions of the ligand with strand 1 of the DNA helix. These changes can be understood by the change in the ligand position that results from the open enediyne structure.

In Figure S1, two planes are constructed to describe the minor groove of DNA. The bottom plane (Figure S1) is defined by the three P atoms of residues THY8, GUA7 and ADE6, which form part of the second strand and lie underneath the ligand. The upper plane is defined by the three P atoms of residues CYT7, THY8 and GUA9, which form part of the first strand, located above the ligand. The angle between the two planes, as indicated in Figure S1, is 150.5^{o}. The formation of **4** results in a slight increase of this angle to 151.2^{o} due to the interaction of the ligand with the backbone atoms of the upper strand. The formation of the more open head unit, present in **4**, results in the wedging of the head unit between two PO_4^- groups and brings the methyl group of the methoxy substituent close to the PO_4^- group (C7) of the backbone.

Figure S1. Change in the position of the ligand [(a) **2**; (b) **4**] relative to the DNA strands. Distances in Å, angles in °.

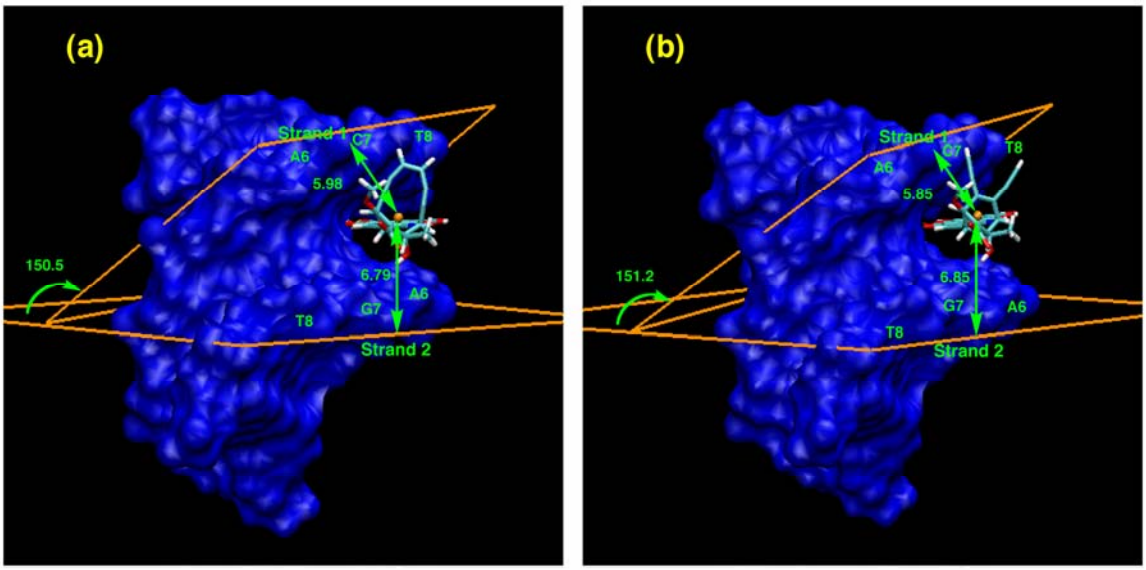

The change in the distance between the geometric center (orange ball in Figure S1) of the ligand and the upper and lower planes indicates the upward movement of the ligand. The distance to the upper plane decreases from 5.98 Å to 5.85 Å (ΔR = -0.13 Å) during formation of **3**, whereas the distance to the lower plane increases from 6.79 Å to 6.85 Å (ΔR = 0.06 Å). Clearly, the open structure of **4** results in a tightly wedged complex, with the ligand being drawn into the DNA minor groove.

The C atoms of the anthraquinone unit of the ligand define an additional plane, which can be used to determine the angle between the ligand and the lower plane of DNA. The angle between this plane (not shown) and the bottom plane is 3.8°, indicating that **1** is essentially parallel to the backbone atoms of the DNA second strand. For the product (**3**) this orientation is essentially conserved with a minor decrease in the angle between the bottom plane and the anthraquinone plane to 3.2°.

3.4 Water energy decomposition. The charge deletion analysis was also applied to the electrostatic interactions between the ligand and the water molecules in the primary

solvent shell (i.e., within 4 Å of the ligand). Table S7 addresses these water molecules, which form H-bonds with the ligand at the specified oxygen acceptor atoms. It lists the variations along the reaction path (relative to **2**) of the associated H-bond energies (ΔΔE as obtained from charge deletion analysis, see main paper) and H-bond lengths (ΔR).

Table S7. The effect of specific H-bonds between the ligand and neighboring water molecules (see text). ΔΔE in kcal/mol, ΔR in Å, both relative to **2.** For atom numbering, see Scheme 1 in the paper.

	ΔΔE / ΔR			
O(acc)	**TS(2-3)**	**3**	**TS(3-4)**	**4**
O1	-0.2/-0.03	-0.5/-0.06	-0.5/-0.07	-0.3/-0.05
O4	-0.1/0.0	-0.2/0.00	-0.1/0.00	0.0/0.00
O5	-0.2/-0.01	-0.4/-0.02	-0.3/-0.03	-1.4/-0.09
O7	-0.2/0.0	-0.2/0.00	-0.2/0.00	-0.2/-0.01
O7	0.2/0.02	0.0/0.01	0.0/0.00	0.3/0.02
O8	0.2/0.01	0.4/0.01	0.7/0.02	0.7/0.02
O8	-0.2/-0.01	-0.1/-0.01	0.0/-0.01	0.0/-0.02
O9	0.2/0.01	0.9/0.03	0.6/0.02	-0.8/0.02

When ΔR is significant (>0.01 Å), the changes ΔΔE correlate well with ΔR. However, generally speaking, the energy changes along the reaction path are rather small and tend to compensate each other. For example, after summing the individual changes, the total effect for **TS(2-3)** is a decrease in the activation barrier by 0.3 kcal/mol.

As pointed out in the main text, H-bonding does not change in the rearrangement of **2** to **4.** This is documented in Figure S2, which compares H-bonding for neutral and anionic dynemicin structures along the reaction path.

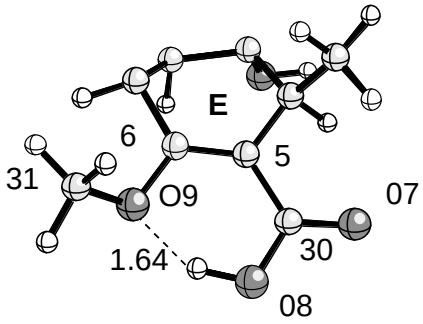

31-O9-6-5 = 133.8
O9 -6-5-30 = -2.7
6-5-30-O7 = -176.1
6-5-30-O8 = 4.1
5-30-O8-H = 0.1

2

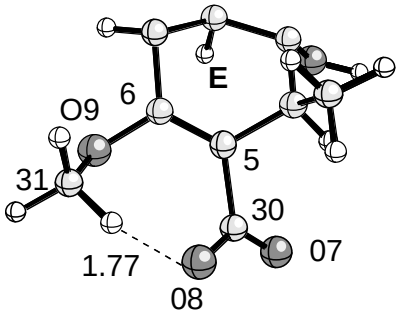

31-O9-6-5 = 71.6
O9 -6-5-30 = -2.7
6-5-30-O7 = 132.3
6-5-30-O8 = -47.5
5-30-O8-H = 25.8

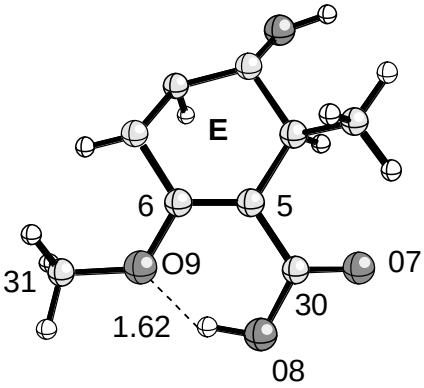

31-O9-6-5 = -171.5
O9 -6-5-30 = 8.8
6-5-30-O7 = 170.6
6-5-30-O8 = -8.6
5-30-O8-H = 1.1

TS(2-3)

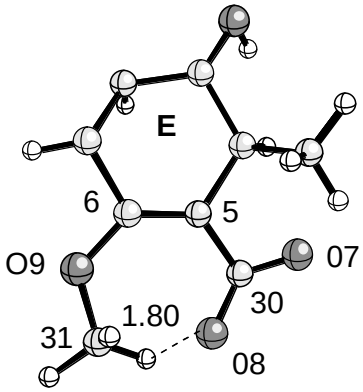

31-O9-6-5 = 39.7
O9 -6-5-30 = 14.6
6-5-30-O7 = 167.9
6-5-30-O8 = -9.7
5-30-O8-H = -27.8

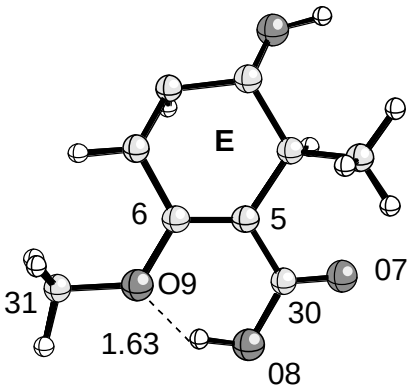

31-O9-6-5 = -172.2
O9 -6-5-30 = 7.5
6-5-30-O7 = 172.6
6-5-30-O8 = -6.8
5-30-O8-H = 0.7

3

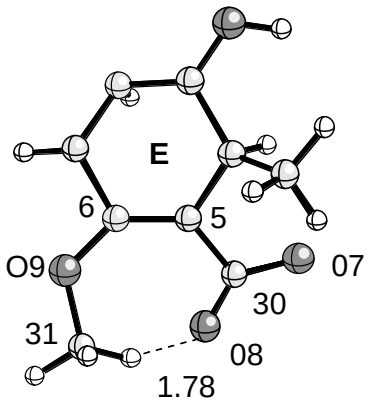

31-O9-6-5 = 30.7
O9 -6-5-30 = 17.4
6-5-30-O7 = 174.9
6-5-30-O8 = -2.4
5-30-O8-H = -33.9

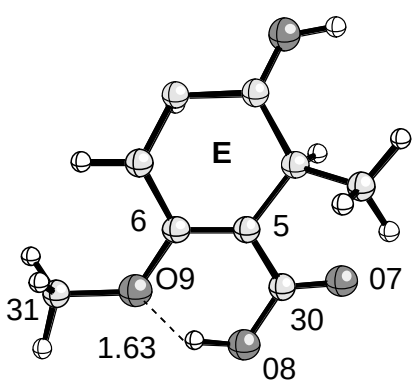

31-O9-6-5 = -178.2
O9 -6-5-30 = 5.9
6-5-30-O7 = 173.9
6-5-30-O8 = -5.5
5-30-O8-H = 0.7

TS(3-4)

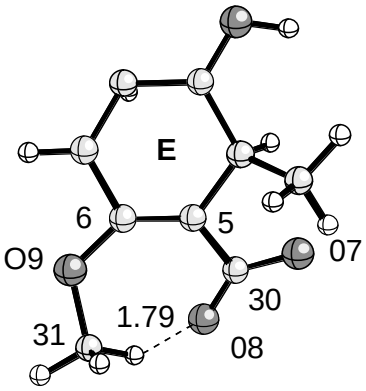

31-O9-6-5 = 31.8
O9 -6-5-30 = 15.8
6-5-30-O7 = 175.6
6-5-30-O8 = -2.1
5-30-O8-H = -33.3

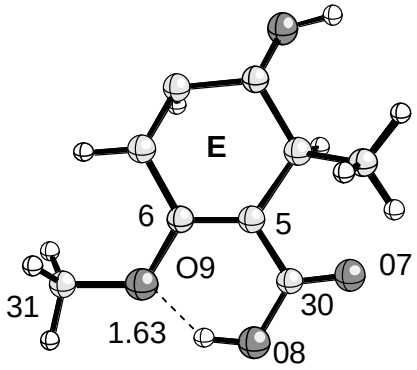

31-O9-6-5 = -161.7
O9 -6-5-30 = 7.2
6-5-30-O7 = 173.0
6-5-30-O8 = -6.5
5-30-O8-H = 0.3

4

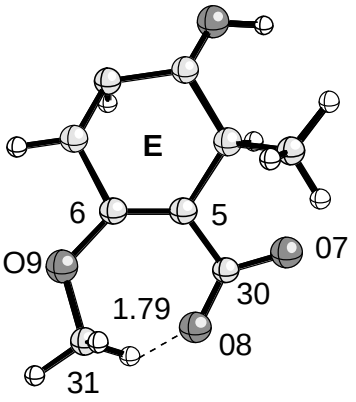

31-O9-6-5 = 34.9
O9 -6-5-30 = 13.4
6-5-30-O7 = 175.5
6-5-30-O8 = -2.3
5-30-O8-H = -32.8

Figure S2. Calculated geometrical parameters for the H-bonds involving the carboxyl and methoxy groups located at ring E.

4. Conformational analysis of rings E and D in dynemicin

Ring F of dynemicin (**2**) is deformed by steric interactions with the back of the minor groove upon an edge-wise insertion into the minor groove between strands 1 and 2, which implies a change of the puckering of rings E and D. In the main paper it is discussed that in the course of the Bergman cyclization ring E converts from a twist-boat form to a half-boat form with lower degree of puckering to give the triple bonds a chance of approaching each other. This is indicated in Figure S3, which schematically describes the deformation of ring E on the conformational globe of a cyclohexene ring when **2** is transferred from the gas phase into the minor groove.

In Figure S4, the numbering system used in Figure S3 is explained by relating atom numbers of Scheme 1 (see main text) to atom numbers used in Figure S3 (clockwise counting for each ring) and presenting the conformations adopted by rings E and D in the minor groove.

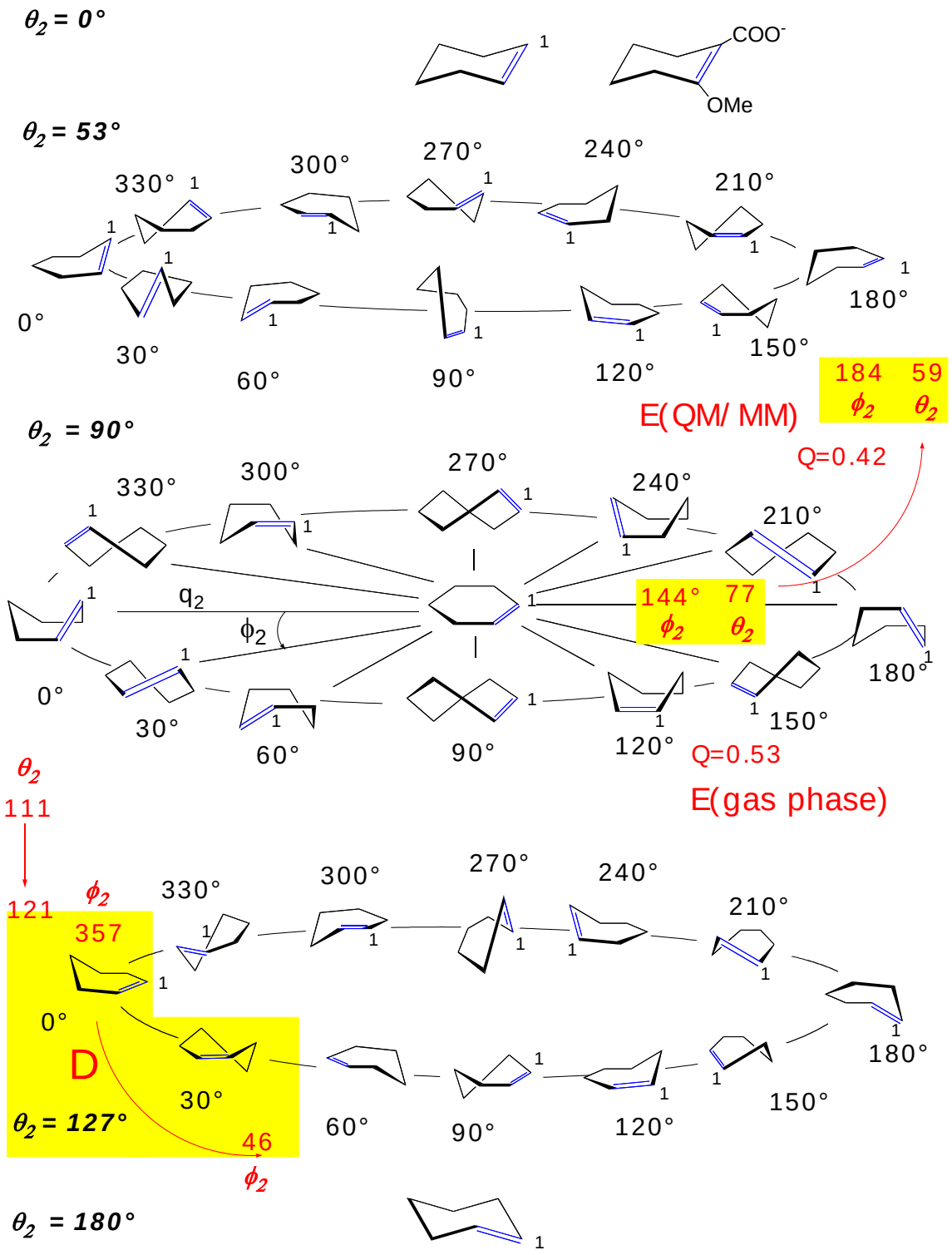
θ2 = 0°
COO-
OMe
θ2 = 53°
330°
300°
270°
240°
210°
180°
150°
120°
90°
60°
30°
0°
184 59
ϕ2 θ2
E(QM/ MM)
θ2 = 90°
Q=0.42
q2
ϕ2
144° 77
ϕ2 θ2
Q=0.53
E(gas phase)
θ2
111
121
ϕ2
357
D
θ2 = 127°
46
ϕ2
θ2 = 180°

Figure S3. Conformational globe of cyclohexene spanned by puckering amplitudes q_2 and q3 and pseudorotational phase angle ϕ_2 (cylindrical coordinate system). Alternatively the spherical coordinate system including the total puckering amplitude Q, the pseudorotational phase angle ϕ_2, and the angle θ_2 can be used. Cyclohexene is the appropriate model for rings E and D of dynemicin **2**. The deformation of these rings when **2** is transferred from the gas phase into the minor groove is indicated.

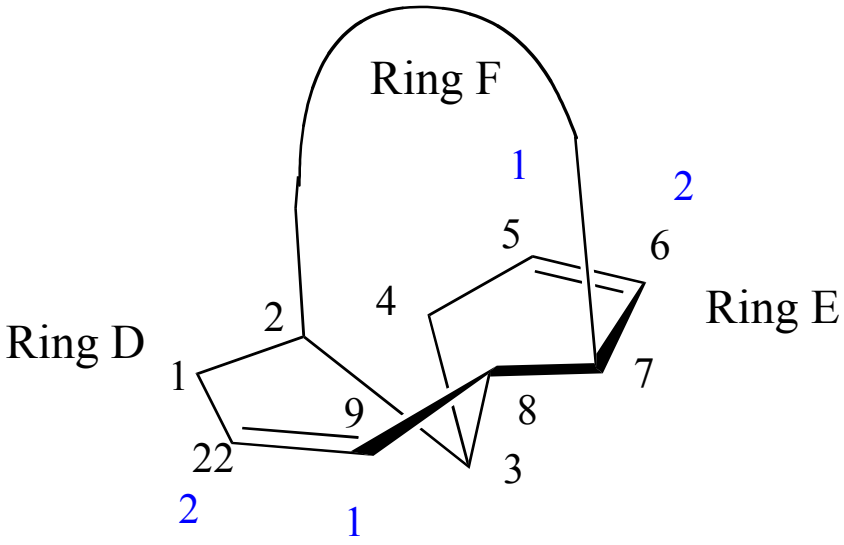

Figure S4. Schematic representation of rings D, E, and F in the conformations adopted in the minor groove. Atom C5 corresponds to 1 in Figure S3 for ring E, atom C9 to 1 in Figure S3 for ring D.

5. CHARMM topology file for dynemicin A.

```
RESI DYNA       -1.000
ATOM N1   NP     -0.400
ATOM C1   CT      0.050
ATOM C2   CT      0.250
ATOM C3   CT     -0.050
ATOM C4   CUA1    0.000
ATOM C5   C       0.150
ATOM C6   CT     -0.050
ATOM C7   CT     -0.050
ATOM C21  C6R     0.050
ATOM C22  CUY1    0.000
ATOM C23  CUY1    0.000
ATOM C24  CUA1   -0.100
ATOM C25  CUA1   -0.100
ATOM C26  CUY1    0.000
ATOM C27  CUY1    0.000
ATOM C28  CT     -0.150
ATOM C29  C       0.200
ATOM C30  CT      0.030
ATOM O1   OT     -0.650
ATOM O7   OC     -0.600
ATOM O8   OC     -0.600
ATOM O9   OE     -0.330
ATOM H4   H       0.250
ATOM H5   HA      0.050
ATOM H6   HA      0.050
ATOM H7   HA      0.050
ATOM H11  HA      0.100
ATOM H12  HA      0.100
ATOM H13  HA      0.050
ATOM H14  HA      0.050
ATOM H15  HA      0.050
ATOM H16  HA      0.050
ATOM H17  HA      0.050
ATOM H18  HA      0.050
ATOM H19  HA      0.050
ATOM H20  HO      0.400
GROUP  !Anthraquinone moiety
ATOM C8   C6R     0.000
ATOM C9   C6R    -0.130
ATOM C10  C6R     0.250
ATOM C11  C6R     0.000
```

```
ATOM C12  C       0.550
ATOM C13  C6R     0.000
ATOM C14  C6R     0.250
ATOM C15  C6R    -0.130
ATOM C16  C6R    -0.130
ATOM C17  C6R     0.250
ATOM C18  C6R     0.000
ATOM C19  C       0.550
ATOM C20  C6R     0.000
ATOM O2   OT     -0.650
ATOM O3   O      -0.550
ATOM O4   OT     -0.650
ATOM O5   OT     -0.650
ATOM O6   O      -0.550
ATOM H1   HO      0.400
ATOM H2   HO      0.400
ATOM H3   HO      0.400
ATOM H8   HA      0.130
ATOM H9   HA      0.130
ATOM H10  HA      0.130
BOND N1   C1
BOND N1   C21
BOND N1   H4
BOND C1   C2
BOND C1   C22
BOND C1   H5
BOND C2   C3
BOND C2   C7
BOND C2   O1
BOND C3   C28
BOND C3   H6
BOND C3   C4
BOND C4   C5
BOND C4   C29
BOND C5   C6
BOND C5   O9
BOND C6   C7
BOND C6   C27
BOND C6   H7
BOND C7   C8
BOND C7   H19
BOND C8   C9
BOND C8   C21
BOND C9   C10
BOND C9   H8
BOND C10  C11
```

BOND C10 O2
BOND C11 C12
BOND C11 C20
BOND C12 C13
BOND C12 O3
BOND C13 C14
BOND C13 C18
BOND C14 C15
BOND C14 O4
BOND C15 C16
BOND C15 H9
BOND C16 C17
BOND C16 H10
BOND C17 C18
BOND C17 O5
BOND C18 C19
BOND C19 C20
BOND C19 O6
BOND C20 C21
BOND C22 C23
BOND C23 C24
BOND C24 C25
BOND C24 H11
BOND C25 C26
BOND C25 H12
BOND C26 C27
BOND C28 H13
BOND C28 H14
BOND C28 H15
BOND C29 O7
BOND C29 O8
BOND C30 O9
BOND C30 H16
BOND C30 H17
BOND C30 H18
BOND H1 O2
BOND H2 O4
BOND H3 O5
BOND O1 H20

6. List of active atoms for the optimized structures.

In this section we list the numbers for the active atoms during the QM/MM optimization of each structure discussed in the paper. The atom numbers are consistent with those in the analogous structure contained in the PDB file. Throughout the course of the reaction the active atom list remained the same.

Active atom list for RRR – 2853 atoms.

1 2 3 4 5 6 7 8 9 10 11 12 13 14 15 16 17 18 19
20 21 22 23 24 25 26 27 28 29 30 31 32 33 34 35 36 37
38 39 40 41 42 43 44 45 46 47 48 49 50 51 52 53 54 55
56 57 58 59 60 61 62 63 64 65 66 67 68 69 70 71 72 73
74 75 76 77 78 79 80 81 82 83 84 85 86 87 88 89 90 91
92 93 94 95 96 97 98 99 100 101 102 103 104 105 106 107 108
109 110 111 112 113 114 115 116 117 118 119 120 121 122 123 124
125 126 127 128 129 130 131 132 133 134 135 136 137 138 139 140
141 142 143 144 145 146 147 148 149 150 151 152 153 154 155 156
157 158 159 160 161 162 163 164 165 166 167 168 169 170 171 172
173 174 175 176 177 178 179 180 181 182 183 184 185 186 187 188
189 190 191 192 193 194 195 196 197 198 199 200 201 202 203 204
205 206 207 208 209 210 211 212 213 214 215 216 217 218 219 220
221 222 223 224 225 226 227 228 229 230 231 232 233 234 235 236
237 238 239 240 241 242 243 244 245 246 247 248 249 250 251 252
253 254 255 256 257 258 259 260 261 262 263 264 265 266 267 268
269 270 271 272 273 274 275 276 277 278 279 280 281 282 283 284
285 286 287 288 289 290 291 292 293 294 295 296 297 298 299 300
301 302 303 304 305 306 307 308 309 310 311 312 313 314 315 316
317 318 319 320 321 322 323 324 325 326 327 328 329 330 331 332
333 334 335 336 337 338 339 340 341 342 343 344 345 346 347 348
349 350 351 352 353 354 355 356 357 358 359 360 361 362 363 364
365 366 367 368 369 370 371 372 373 374 375 376 377 378 379 380
381 382 383 384 385 386 387 388 389 390 391 392 393 394 395 396
397 398 399 400 401 402 403 404 405 406 407 408 409 410 411 412
413 414 415 416 417 418 419 420 421 422 423 424 425 426 427 428
429 430 431 432 433 434 435 436 437 438 439 440 441 442 443 444
445 446 447 448 449 450 451 452 453 454 455 456 457 458 459 460
461 462 463 464 465 466 467 468 469 470 471 472 473 474 475 476
477 478 479 480 481 482 483 484 485 486 487 488 489 490 491 492
493 494 495 496 497 498 499 500 501 502 503 504 505 506 507 508
509 510 511 512 513 514 515 516 517 518 519 520 521 522 523 524
525 526 527 528 529 530 531 532 533 534 535 536 537 538 539 540

541 542 543 544 545 546 547 548 549 550 551 552 553 554 555 556
557 558 559 560 561 562 563 564 565 566 567 568 569 570 571 572
573 574 575 576 577 578 579 580 581 582 583 584 585 586 587 588
589 590 591 592 593 594 595 596 597 598 599 600 601 602 640 641
642 643 644 645 646 647 648 649 650 651 652 653 654 655 656 657
658 659 660 661 662 663 664 665 666 667 668 669 670 671 672 673
674 675 676 677 678 679 680 681 682 683 684 685 686 687 688 689
690 691 692 693 694 695 696 697 698 699 706 707 708 709 710 711
727 728 729 757 758 759 760 761 762 778 779 780 823 824 825 826
827 828 841 842 843 865 866 867 868 869 870 883 884 885 886 887
888 913 914 915 916 917 918 922 923 924 964 965 966 1012 1013 1014
1033 1034 1035 1051 1052 1053 1060 1061 1062 1063 1064 1065 1072 1073
1074 1078 1079 1080 1102 1103 1104 1105 1106 1107 1114 1115 1116 1120
1121 1122 1156 1157 1158 1159 1160 1161 1165 1166 1167 1177 1178 1179
1195 1196 1197 1198 1199 1200 1216 1217 1218 1222 1223 1224 1249 1250
1251 1255 1256 1257 1285 1286 1287 1288 1289 1290 1297 1298 1299 1309
1310 1311 1342 1343 1344 1348 1349 1350 1375 1376 1377 1378 1379 1380
1396 1397 1398 1432 1433 1434 1435 1436 1437 1441 1442 1443 1456 1457
1458 1471 1472 1473 1483 1484 1485 1486 1487 1488 1492 1493 1494 1495
1496 1497 1504 1505 1506 1528 1529 1530 1531 1532 1533 1543 1544 1545
1549 1550 1551 1573 1574 1575 1576 1577 1578 1582 1583 1584 1621 1622
1623 1627 1628 1629 1630 1631 1632 1639 1640 1641 1645 1646 1647 1669
1670 1671 1672 1673 1674 1678 1679 1680 1714 1715 1716 1717 1718 1719
1723 1724 1725 1756 1757 1758 1759 1760 1761 1765 1766 1767 1783 1784
1785 1795 1796 1797 1804 1805 1806 1807 1808 1809 1816 1817 1818 1822
1823 1824 1825 1826 1827 1846 1847 1848 1849 1850 1851 1855 1856 1857
1858 1859 1860 1867 1868 1869 1873 1874 1875 1885 1886 1887 1906 1907
1908 1912 1913 1914 1942 1943 1944 1948 1949 1950 1951 1952 1953 1960
1961 1962 1966 1967 1968 1969 1970 1971 1996 1997 1998 1999 2000 2001
2014 2015 2016 2017 2018 2019 2038 2039 2040 2044 2045 2046 2047 2048
2049 2092 2093 2094 2110 2111 2112 2140 2141 2142 2161 2162 2163 2170
2171 2172 2200 2201 2202 2203 2204 2205 2215 2216 2217 2242 2243 2244
2245 2246 2247 2263 2264 2265 2287 2288 2289 2290 2291 2292 2308 2309
2310 2311 2312 2313 2338 2339 2340 2350 2351 2352 2356 2357 2358 2395
2396 2397 2398 2399 2400 2404 2405 2406 2410 2411 2412 2446 2447 2448
2449 2450 2451 2464 2465 2466 2497 2498 2499 2506 2507 2508 2509 2510
2511 2518 2519 2520 2524 2525 2526 2527 2528 2529 2554 2555 2556 2560
2561 2562 2566 2567 2568 2599 2600 2601 2602 2603 2604 2620 2621 2622
2653 2654 2655 2659 2660 2661 2665 2666 2667 2686 2687 2688 2689 2690
2691 2695 2696 2697 2701 2702 2703 2782 2783 2784 2788 2789 2790 2812
2813 2814 2818 2819 2820 2833 2834 2835 2845 2846 2847 2869 2870 2871
2890 2891 2892 2899 2900 2901 2914 2915 2916 2935 2936 2937 2938 2939
2940 2944 2945 2946 2959 2960 2961 2977 2978 2979 2983 2984 2985 2986
2987 2988 2998 2999 3000 3004 3005 3006 3028 3029 3030 3034 3035 3036
3040 3041 3042 3043 3044 3045 3067 3068 3069 3073 3074 3075 3082 3083
3084 3088 3089 3090 3115 3116 3117 3118 3119 3120 3124 3125 3126 3154

3155 3156 3160 3161 3162 3172 3173 3174 3196 3197 3198 3202 3203 3204
3205 3206 3207 3217 3218 3219 3220 3221 3222 3247 3248 3249 3250 3251
3252 3256 3257 3258 3268 3269 3270 3274 3275 3276 3295 3296 3297 3304
3305 3306 3316 3317 3318 3343 3344 3345 3346 3347 3348 3352 3353 3354
3379 3380 3381 3385 3386 3387 3394 3395 3396 3400 3401 3402 3424 3425
3426 3427 3428 3429 3433 3434 3435 3445 3446 3447 3451 3452 3453 3472
3473 3474 3511 3512 3513 3529 3530 3531 3532 3533 3534 3541 3542 3543
3556 3557 3558 3571 3572 3573 3574 3575 3576 3580 3581 3582 3619 3620
3621 3652 3653 3654 3655 3656 3657 3673 3674 3675 3700 3701 3702 3718
3719 3720 3724 3725 3726 3745 3746 3747 3766 3767 3768 3805 3806 3807
3808 3809 3810 3814 3815 3816 3829 3830 3831 3844 3845 3846 3862 3863
3864 3871 3872 3873 3895 3896 3897 3898 3899 3900 3904 3905 3906 3943
3944 3945 3964 3965 3966 3979 3980 3981 3982 3983 3984 4000 4001 4002
4003 4004 4005 4009 4010 4011 4030 4031 4032 4033 4034 4035 4051 4052
4053 4057 4058 4059 4090 4091 4092 4120 4121 4122 4138 4139 4140 4171
4172 4173 4174 4175 4176 4180 4181 4182 4192 4193 4194 4198 4199 4200
4213 4214 4215 4228 4229 4230 4234 4235 4236 4258 4259 4260 4267 4268
4269 4273 4274 4275 4300 4301 4302 4306 4307 4308 4333 4334 4335 4336
4337 4338 4354 4355 4356 4393 4394 4395 4399 4400 4401 4411 4412 4413
4426 4427 4428 4447 4448 4449 4450 4451 4452 4456 4457 4458 4486 4487
4488 4498 4499 4500 4504 4505 4506 4537 4538 4539 4540 4541 4542 4558
4559 4560 4561 4562 4563 4582 4583 4584 4588 4589 4590 4600 4601 4602
4603 4604 4605 4609 4610 4611 4630 4631 4632 4639 4640 4641 4648 4649
4650 4651 4652 4653 4684 4685 4686 4687 4688 4689 4702 4703 4704 4708
4709 4710 4729 4730 4731 4735 4736 4737 4774 4775 4776 4786 4787 4788
4792 4793 4794 4825 4826 4827 4831 4832 4833 4837 4838 4839 4858 4859
4860 4876 4877 4878 4882 4883 4884 4906 4907 4908 4912 4913 4914 4924
4925 4926 4930 4931 4932 4963 4964 4965 4966 4967 4968 4999 5000 5001
5005 5006 5007 5020 5021 5022 5038 5039 5040 5044 5045 5046 5047 5048
5049 5062 5063 5064 5065 5066 5067 5092 5093 5094 5095 5096 5097 5116
5117 5118 5143 5144 5145 5152 5153 5154 5158 5159 5160 5194 5195 5196
5200 5201 5202 5206 5207 5208 5233 5234 5235 5236 5237 5238 5248 5249
5250 5254 5255 5256 5284 5285 5286 5290 5291 5292 5296 5297 5298 5338
5339 5340 5344 5345 5346 5377 5378 5379 5380 5381 5382 5389 5390 5391
5395 5396 5397 5398 5399 5400 5419 5420 5421 5425 5426 5427 5440 5441
5442 5461 5462 5463 5467 5468 5469 5470 5471 5472 5479 5480 5481 5485
5486 5487 5509 5510 5511 5524 5525 5526 5533 5534 5535 5557 5558 5559
5560 5561 5562 5566 5567 5568 5569 5570 5571 5578 5579 5580 5593 5594
5595 5599 5600 5601 5602 5603 5604 5620 5621 5622 5644 5645 5646 5647
5648 5649 5653 5654 5655 5689 5690 5691 5728 5729 5730 5737 5738 5739
5743 5744 5745 5773 5774 5775 5779 5780 5781 5809 5810 5811 5818 5819
5820 5830 5831 5832 5836 5837 5838 5854 5855 5856 5857 5858 5859 5863
5864 5865 5875 5876 5877 5896 5897 5898 5902 5903 5904 5911 5912 5913
5917 5918 5919 5941 5942 5943 5959 5960 5961 5986 5987 5988 6004 6005
6006 6007 6008 6009 6013 6014 6015 6034 6035 6036 6037 6038 6039 6043
6044 6045 6052 6053 6054 6058 6059 6060 6082 6083 6084 6091 6092 6093

6112 6113 6114 6130 6131 6132 6154 6155 6156 6157 6158 6159 6163 6164
6165 6175 6176 6177 6181 6182 6183 6199 6200 6201 6223 6224 6225 6250
6251 6252 6253 6254 6255 6295 6296 6297 6301 6302 6303 6316 6317 6318
6328 6329 6330 6331 6332 6333 6337 6338 6339 6340 6341 6342 6349 6350
6351 6355 6356 6357 6358 6359 6360 6382 6383 6384 6385 6386 6387 6391
6392 6393 6394 6395 6396 6427 6428 6429 6430 6431 6432 6436 6437 6438
6475 6476 6477 6490 6491 6492 6496 6497 6498 6511 6512 6513 6541 6542
6543 6547 6548 6549 6580 6581 6582 6586 6587 6588 6595 6596 6597 6622
6623 6624 6628 6629 6630 6673 6674 6675 6679 6680 6681 6712 6713 6714
6718 6719 6720 6724 6725 6726 6727 6728 6729 6763 6764 6765 6769 6770
6771 6778 6779 6780 6814 6815 6816 6826 6827 6828 6859 6860 6861 6865
6866 6867 6868 6869 6870 6880 6881 6882 6886 6887 6888 6913 6914 6915
6919 6920 6921 6925 6926 6927 6934 6935 6936 6949 6950 6951 6964 6965
6966 6970 6971 6972 6994 6995 6996 7009 7010 7011 7015 7016 7017 7045
7046 7047 7063 7064 7065 7072 7073 7074 7102 7103 7104 7129 7130 7131
7150 7151 7152 7156 7157 7158 7192 7193 7194 7210 7211 7212 7216 7217
7218 7240 7241 7242 7258 7259 7260 7261 7262 7263 7267 7268 7269 7291
7292 7293 7306 7307 7308 7345 7346 7347 7351 7352 7353 7366 7367 7368
7375 7376 7377 7399 7400 7401 7402 7403 7404 7414 7415 7416 7438 7439
7440 7459 7460 7461 7465 7466 7467 7489 7490 7491 7504 7505 7506 7528
7529 7530 7549 7550 7551 7555 7556 7557 7570 7571 7572 7576 7577 7578
7591 7592 7593 7609 7610 7611 7615 7616 7617 7630 7631 7632 7636 7637
7638 7666 7667 7668 7672 7673 7674 7684 7685 7686 7696 7697 7698 7702
7703 7704 7732 7733 7734 7756 7757 7758 7771 7772 7773 7777 7778 7779
7816 7817 7818 7822 7823 7824 7843 7844 7845 7861 7862 7863 7867 7868
7869 7879 7880 7881 7888 7889 7890 7906 7907 7908 7909 7910 7911 7915
7916 7917 7918 7919 7920 7936 7937 7938 7951 7952 7953 7954 7955 7956
7960 7961 7962 7963 7964 7965 7972 7973 7974 7981 7982 7983 7996 7997
7998 8005 8006 8007 8008 8009 8010 8017 8018 8019 8026 8027 8028 8041
8042 8043 8083 8084 8085 8089 8090 8091 8092 8093 8094 8131 8132 8133
8146 8147 8148 8164 8165 8166 8173 8174 8175 8191 8192 8193 8194 8195
8196 8209 8210 8211 8218 8219 8220 8221 8222 8223 8230 8231 8232 8236
8237 8238 8257 8258 8259 8263 8264 8265 8266 8267 8268 8272 8273 8274
8305 8306 8307 8326 8327 8328 8344 8345 8346 8350 8351 8352 8362 8363
8364 8389 8390 8391 8407 8408 8409 8431 8432 8433 8437 8438 8439 8449
8450 8451 8452 8453 8454 8479 8480 8481 8485 8486 8487 8497 8498 8499
8518 8519 8520 8524 8525 8526 8539 8540 8541 8545 8546 8547 8563 8564
8565 8566 8567 8568 8581 8582 8583 8602 8603 8604 8608 8609 8610 8623
8624 8625 8647 8648 8649 8650 8651 8652 8656 8657 8658 8668 8669 8670
8695 8696 8697 8698 8699 8700 8704 8705 8706 8716 8717 8718 8728 8729
8730 8737 8738 8739 8740 8741 8742 8749 8750 8751 8752 8753 8754 8767
8768 8769 8770 8771 8772 8776 8777 8778 8797 8798 8799 8800 8801 8802
8806 8807 8808 8839 8840 8841 8857 8858 8859 8881 8882 8883 8884 8885
8886 8899 8900 8901 8905 8906 8907 8923 8924 8925 8941 8942 8943 8944
8945 8946 8959 8960 8961 8977 8978 8979 8986 8987 8988 8995 8996 8997
8998 8999 9000 9004 9005 9006 9007 9008 9009 9019 9020 9021 9022 9023

9024 9043 9044 9045 9046 9047 9048 9052 9053 9054 9055 9056 9057 9064
9065 9066 9073 9074 9075 9085 9086 9087 9103 9104 9105 9130 9131 9132
9163 9164 9165 9169 9170 9171 9175 9176 9177 9205 9206 9207 9211 9212
9213 9220 9221 9222 9226 9227 9228 9247 9248 9249 9250 9251 9252 9256
9257 9258 9265 9266 9267 9271 9272 9273 9292 9293 9294 9295 9296 9297
9301 9302 9303 9310 9311 9312 9319 9320 9321 9343 9344 9345 9346 9347
9348 9376 9377 9378 9385 9386 9387 9397 9398 9399 9403 9404 9405 9424
9425 9426 9433 9434 9435 9442 9443 9444 9448 9449 9450 9451 9452 9453
9472 9473 9474 9475 9476 9477 9481 9482 9483 9484 9485 9486 9493 9494
9495 9499 9500 9501 9502 9503 9504 9523 9524 9525 9526 9527 9528 9532
9533 9534 9568 9569 9570 9571 9572 9573 9577 9578 9579 9610 9611 9612
9619 9620 9621 9622 9623 9624 9628 9629 9630 9655 9656 9657 9658 9659
9660 9676 9677 9678 9682 9683 9684 9703 9704 9705 9706 9707 9708 9712
9713 9714 9715 9716 9717 9724 9725 9726 9730 9731 9732 9751 9752 9753
9754 9755 9756 9760 9761 9762 9763 9764 9765 9775 9776 9777 9805 9806
9807 9808 9809 9810 9814 9815 9816 9826 9827 9828 9850 9851 9852 9865
9866 9867 9874 9875 9876 9880 9881 9882 9895 9896 9897 9901 9902 9903
9928 9929 9930 9931 9932 9933 9937 9938 9939 9940 9941 9942 9949 9950
9951 9955 9956 9957 9970 9971 9972 9973 9974 9975 9982 9983 9984 9991
9992 9993 10000 10001 10002 10024 10025 10026 10027 10028 10029 10033 10034
10035 10054 10055 10056 10081 10082 10083 10087 10088 10089 10108 10109 10110
10126 10127 10128 10150 10151 10152 10156 10157 10158 10189 10190 10191 10195
10196 10197 10198 10199 10200 10216 10217 10218 10246 10247 10248 10249 10250
10251 10300 10301 10302 10330 10331 10332 10336 10337 10338 10357 10358 10359
10363 10364 10365 10372 10373 10374 10378 10379 10380 10399 10400 10401 10405
10406 10407 10417 10418 10419 10451 10452 10453 10454 10455 10460 10461 10462
10463 10464

7. PDB coordinates for QM/MM optimized structures.

The PDB coordinates (in a separate PDB file) correspond to the final QM/MM optimized geometry of each structure discussed in the paper.